Journal of Materials Chemistry C

RSC Publishing

PAPER

View Article Online
View Journal | View Issue

Cite this: *J. Mater. Chem. C*, 2013, **1**, 5402

Enhanced charge extraction of polymer solar cell by solution-processable gold nanoparticles†

Si Yun Khoo,[ab] Hongbin Yang,[a] Ziming He,[a] Jianwei Miao,[a] Kam Chew Leong,[b] Chang Ming Li*[c] and Timothy Thatt Yang Tan*[a]

Received 21st May 2013
Accepted 29th June 2013

DOI: 10.1039/c3tc30956h

www.rsc.org/MaterialsC

The utilization of metallic nanoparticles is one of the key strategies to improve the performance of photovoltaic devices. In this work, we elucidate the power conversion efficiency (PCE) enhancement mechanism by gold nanoparticles (Au-NPs) through a bilayer anodic buffer structure in polymer solar cells. The results show that the PCE of the device based on a Au-NP:poly(sodium-4-styrenesulfonate)/V_2O_5 bilayer buffer exhibits a ~16% enhancement compared with the device without Au-NP. By controlling the density of Au-NPs to minimize plasmonic effects, the Au-NP induced enhancement of charge extraction and crystallinity of the photoactive layer were demonstrated for the first time. Our work indicates that the plasmonic effect may not be the only factor that enhances the PCE of polymer solar cells, while providing new insights into the roles of Au-NPs in performance improvement of a bulk-heterojunction polymer solar cell.

Introduction

Bulk-heterojunction polymer solar cells, with their interpenetrating network of electron donors and electron acceptors, have received much attention as promising candidates for sustainable energy due to their low manufacturing costs, scalable fabrication process, flexible substrate and low processing temperature.[1–3] The recent development of novel low band-gap photoactive material and the optimization of the photoactive layer morphology[4–7] have improved the power conversion efficiency (PCE) of polymer solar cells to over 9%.[8] Apart from charge transfer improvement due to the novel interfacial layer,[9,10] incorporating noble metallic nanoparticles in the device architecture to enhance light harvesting is also a strategy to improve the performance of polymer solar cells. Interfacial layers play an important role in reducing charge injection or extraction barriers and result in the formation of ohmic contact between the two conducting electrodes and polymer active layer interfaces.[11–13] Noble metallic nanoparticles, which are well known for their strong interactions with electromagnetic waves due to the localized surface plasmon resonances (LSPR), have been used to increase the light harvesting and current density of photovoltaic cells.[14–18] In particular, gold nanoparticles (Au-NPs) have been shown to cause a significant enhancement in solar cell performance due to their collective oscillations of surface electrons induced by visible light at around 500 nm, which overlaps with the absorption of the active layer of polymer solar cells.[19]

There is no shortage of good studies on the understanding of LSPR in polymer solar cells.[20,21] Wu *et al.* performed an in-depth investigation on the LSPR contribution from Au-NPs towards P3HT:$PC_{61}BM$ based polymer solar cells. The work by Kim *et al.* demonstrated significant enhancement in external quantum efficiency for polymer solar cells using plasmonic noble metal nanoparticles.[17] However, the LSPR effect from Au-NPs might not be the only factor that increases the PCE of polymer solar cells. Heeger *et al.* exemplified an increase in PCE through light scattering activities caused by incorporated Au-NPs.[22]

Here, we design a Au-NP/poly(sodium-4-styrenesulfonate)/V_2O_5 (Au-NP:PSS/V_2O_5) bilayer anodic buffer to enhance the PCE of polymer solar cells. Our results show that a ~16% improvement in the PCE was achieved through the utilization of a Au-NP:PSS/V_2O_5 bilayer anodic buffer. The enhancement mechanisms induced by the Au-NP layer were investigated by analysis of the electrical characteristics of the devices, optical properties and the crystalline structure of the polymer active layers. The current results indicate that the Au-NP:PSS/V_2O_5 bilayer significantly enhances the device efficiency by improving the crystallinity of the active layer and enhancing the charge extraction of the polymer solar cell.

[a]*School of Chemical and Biomedical Engineering, Nanyang Technological University, 62 Nanyang Drive, Singapore 637459. E-mail: tytan@ntu.edu.sg; Fax: +65 6794 7553; Tel: +65 6316 8829*

[b]*Globalfoundries Singapore Pte. Ltd, 60 Woodlands Industrial Park D, Street 2, Singapore 738406, Singapore*

[c]*Institute for Clean Energy and Advanced Materials, Southwest University, Chongqing 400715, China. E-mail: ecmli@swu.edu.cn*

† Electronic supplementary information (ESI) available: AFM topography of blank ITO substrate, supplementary figures of *J–V* curves for the PSS/V_2O_5 bilayer structure devices and table summarizing the device performance with the PSS/V_2O_5 bilayer structure. See DOI: 10.1039/c3tc30956h

Experimental details

Chemicals

Tetrachloroauric acid trihyrate ($AuHCl_4 \cdot 3H_2O$), sodium tricitrate, regioregular poly(3-hexylthiophene) (P3HT), phenyl C_{61}-butyric acid methyl ester ($PC_{61}BM$), poly(sodium-4-styrenesulfonate) (PSS), vanadium oxytriisopropoxide, and chlorobenzene were purchased from Sigma-Aldrich. Isopropanol was supplied from Fisher Scientific. All chemicals were used as purchased without further purification processes.

Preparation of gold nanoparticles

Au-NP colloid was synthesized using a modified Turkevitch method.[23] In brief, a 2.5×10^{-4} M tetrachloroauric acid trihydrate ($AuHCl_4 \cdot 3H_2O$) solution was heated to boiling point, and then 1 ml of sodium tricitrate was injected rapidly into the solution. The gold precursor underwent a reduction process from gold ions to Au-NPs, which was indicated by the change of the solution colour from light yellow to wine reddish within 10 minutes.

Fabrication of polymer solar devices

The devices were fabricated using regioregular poly(3-hexylthiophene):phenyl C_{61}-butyric acid methyl ester (P3HT:$PC_{61}BM$) blend, and the device architecture is depicted in Fig. 1. Before the device fabrication process, transparent patterned conductive glasses (indium-doped tin oxide (ITO), 15 $\Omega\ \square^{-1}$) were cleaned thoroughly by sonication in 5% detergent for 30 min first and then rinsed with de-ionized water (DI water) several times, followed by sonication in DI water for 15 min. This step was repeated twice. The pre-cleaned patterned ITO glasses were dried using nitrogen gas and heated on a 70 °C hotplate for 10 min.

The dried ITO glasses were further cleaned with UV ozone plasma for 20 min to remove any residual organic molecules. A solution of 0.2 wt% poly(sodium-4-styrenesulfonate) (PSS) mixed with Au-NPs (denoted as Au-NP:PSS) was first coated onto the ITO/glass substrate at 5000 rpm for 60 s (~16 nm thick) and heated on a 150 °C hot plate for 30 min. Afterwards, vanadium oxytriisopropoxide was diluted with iso-propanol solvent at 1 : 150 volume ratio and spin coated on the patterned ITO/glass substrate at 8000 rpm for 30 s (~10 nm thick). It is speculated that the possibility of intermixing of Au-NP:PSS with the V_2O_5 layer would be minimal because the Au-NP:PSS layer was heated on the hotplate first to ensure that the layer was dried before the V_2O_5 layer was spin coated onto it. The as-prepared sample was maintained at ambient conditions for 1 h for hydrolysis to take place. Then, a 10 mg ml^{-1} P3HT:$PC_{61}BM$ (both purchased from Sigma-Aldrich) blend (1 : 1 weight ratio) in chlorobenzene was sonicated for 5 min before spin coating at 800 rpm for 25 s on the as-prepared ITO substrate and capped in a chlorobenzene-rich petri dish for 20 min. The photoactive device structures were completed by thermally evaporating 100 nm Al electrodes in a base pressure of 1.0×10^{-5} Pa with a shadow mask to define the active device area. The fabricated solar cells were annealed at 150 °C for 30 min. For the control devices, a polymer solar cell without the Au-NP:PSS layer was fabricated using the conditions described previously. All the processes were carried out under ambient conditions at room temperature except the aluminum electrode deposit process and the annealing process.

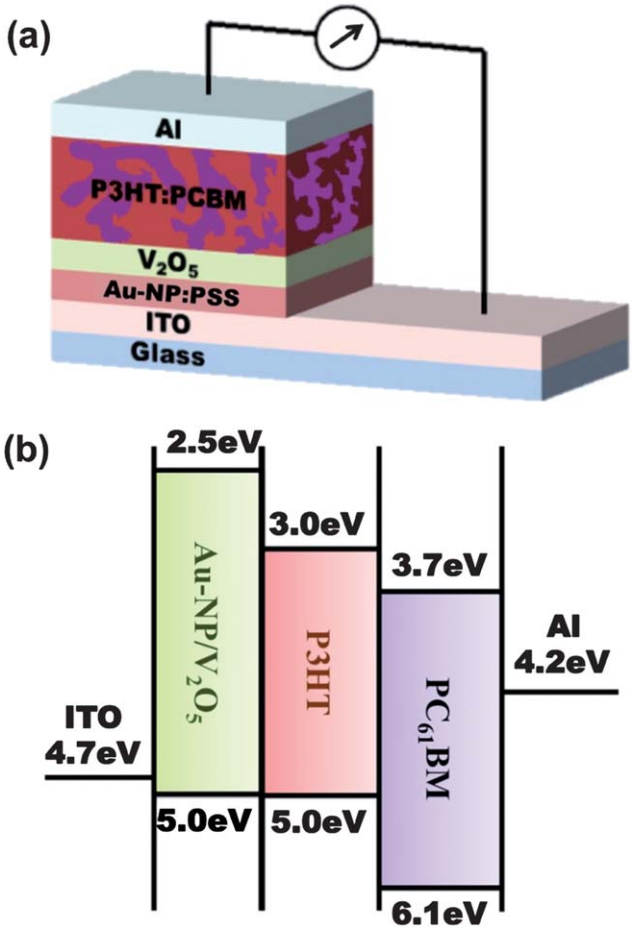

Fig. 1 (a) The device architecture of the conventional polymer solar cell used in this work, *i.e.* ITO/Au-NP:PSS/V_2O_5/P3HT:$PC_{61}BM$/Al, and (b) the band alignment of the components used in the device.

Characterization of the samples

The current density (J) *versus* voltage (V) characteristics were recorded on a Keithley model 2400 source measuring unit in the dark and under illumination by a Newport solar simulator with a 100 mW cm^{-2} AM1.5G spectrum. The intensity of the solar simulator was calibrated by a standard Si photovoltaic cell. Au-NP:PSS on the ITO substrate was observed using a field-effect scanning electrode microscope (FESEM) (JEOL JSM-6700). The ITO, Au-NPs on ITO, and P3HT:$PC_{61}BM$ surface topographies and phase diagrams were observed with an atomic force microscope (AFM Asylum Research, MFP-3D). Solution-based zeta-potential measurements was examined using a zeta-potential analyzer (Nano-ZS Zetasizer with DTS Nanosoftware, Malvern Instruments). The crystallinity of the fabricated devices was studied using an X-ray diffraction (XRD) Rikaku Rint-2000 instrument with Cu Kα radiation ($\lambda = 1.54056$ Å). The absorption spectra were studied using ultraviolet (UV)-visible spectroscopy (Shimadzu UV-2450).

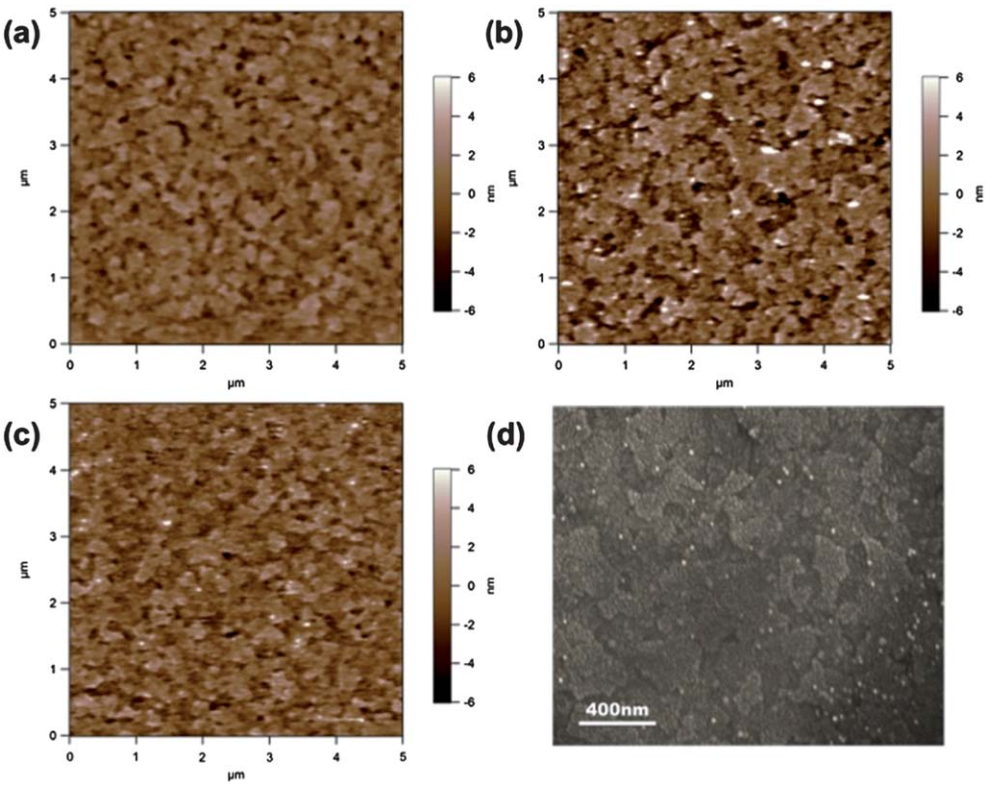

Fig. 2 AFM topography images of (a) V_2O_5, (b) Au-NP/V_2O_5, (c) Au-NP:PSS/V_2O_5 on the ITO substrate and (d) SEM image of Au-NP:PSS coated ITO/glass substrate.

Results and discussions

The solution processed Au-NP was spin-coated onto the ITO substrate using the as-synthesized Au-NP solution (Au-NP) or PSS premixed Au-NP solution (Au-NP:PSS). The surface morphologies of various buffer modified ITO substrates were measured by tapping-mode AFM and the corresponding tilted AFM images are shown in the supporting information (Fig. S2†). Fig. 2(a) shows a very smooth surface of the V_2O_5 covered ITO substrate, with RMS roughness of 1.26 nm, indicating that the V_2O_5 layer planarizes the original rough ITO surface (Fig. S1†) remarkably, which is in agreement with previously reported results.[24] In contrast, spikes were observed on the surface of ITO/Au-NP/V_2O_5 structure (Fig. 2(b)), which resulted from the additional Au-NP layer. The size of the spikes ranged from 20 nm to 100 nm, indicating a non-uniform distribution and significant agglomeration of the Au-NP layer on the ITO surface by spin-coating the citrate-capped Au-NP solution. This result implies that sodium tricitrate, which acts as a reducing agent as well as a capping agent,[25] is not sufficient to prevent the aggregation of Au-NPs. In order to obtain a more uniform distribution of Au-NPs on the ITO surface, the more negatively charged PSS was added into the Au-NP solution.[26,27] As shown in Fig. 2(c), a smaller spike height with a higher density and uniformity of Au-NPs were obtained for the samples prepared from the Au-NP:PSS solution. The improved uniformity could be attributed to the stronger repulsive forces due to mixing the more negatively-charged PSS with the citrate-capped Au-NP solution. The stronger repulsive force was confirmed with the zeta potential measurement, which changes from −45.9 mV to −49 mV for the Au-NP solution and Au-NP:PSS solution, respectively. A higher zeta potential indicates that a larger repulsive force is experienced in the system, which creates an energy barrier that prevents two particles approaching and adhering to each other and causes a more uniform distribution of Au-NPs. The average diameters of the spikes in Fig. 2(c) are around 20 nm, which is in good agreement with the SEM image of the Au-NP:PSS coated ITO substrate as shown in Fig. 2(d).

The *J*–*V* characteristics of the illuminated polymer solar cells with different anodic buffer layers are shown in Fig. 3(a) and the solar cell performance parameters are summarized in Table 1. As displayed in Table 1, the reference device prepared with the V_2O_5 buffer layer (V_2O_5) exhibits a short-circuit current density (J_{sc}) of 7.02 mA cm^{-2}, an open-circuit voltage (V_{oc}) of 0.596 V, a fill factor (FF) of 50.5%, and a calculated power conversion efficiency (PCE) of 2.11%. Compared with the reference device, the insertion of Au-NP (Au-NP/V_2O_5) from as-synthesized Au-NP solution does not enhance the performance of the solar cell effectively. As is evident from the lower V_{oc} and J_{sc} values, the decrease in device performance could be attributed to a large amount of charge recombination induced by aggregated Au-NPs at interface between the ITO and V_2O_5 layer. On the other hand, PCE enhancement by ~16% is observed for the polymer solar cell with Au-NP:PSS and a V_2O_5 bilayer structure (Au-NP:PSS/V_2O_5). The PCE improvement mainly originates from the enhancement in the fill factor, which increases from 50.5% to

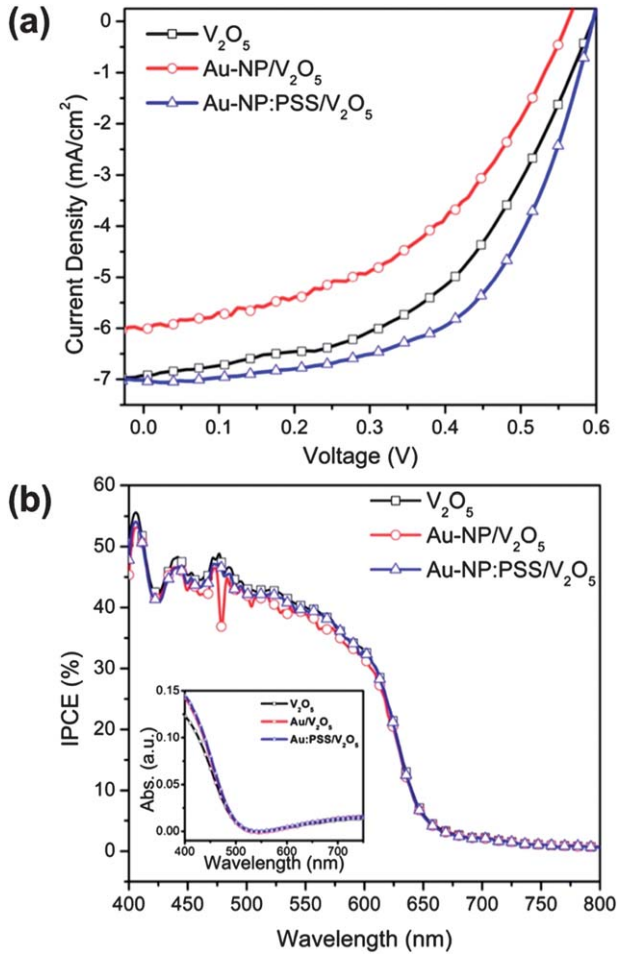

Fig. 3 (a) Current density–voltage (*J–V*) characteristics under AM1.5G illumination for photovoltaic measurements and (b) incident photon-to-current efficiency (IPCE) of polymer solar devices with (black) V_2O_5, (red) Au-NP/V_2O_5 and (blue) Au-NP:PSS/V_2O_5 buffer layer. Inset: UV-visible absorption spectrum of (black) V_2O_5, (red) Au-NP/V_2O_5, and (blue) Au-NP:PSS/V_2O_5 buffer layer.

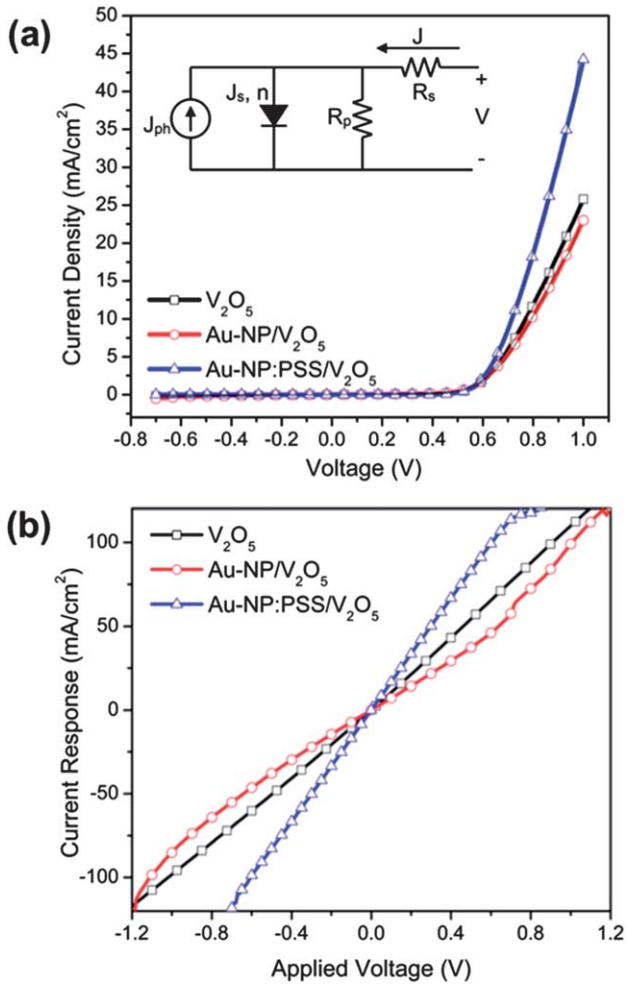

Fig. 4 (a) Dark current response–voltage (*J–V*) characteristics of polymer solar devices with (black) V_2O_5, (red) Au-NP/V_2O_5 and (blue) Au-NP:PSS/V_2O_5 buffer layers and (b) current–voltage characteristics of hole-only devices with (black) V_2O_5, (red) Au-NP/V_2O_5 and (blue) Au-NP:PSS/V_2O_5 buffer layers under dark conditions. The inset in (a) shows the equivalent circuit model used to obtain the values of the circuit elements.

Table 1 Summary of performance parameters of P3HT:$PC_{61}BM$ solar cells fabricated using various buffer layers

Buffer layer	V_{oc} (V)	J_{sc} (mA cm^{-2})	PCE (%)	FF (%)
V_2O_5	0.596	7.02	2.11	50.5
Au-NP/V_2O_5[a]	0.562	6.08	1.57	46.1
Au-NP:PSS[b]/V_2O_5	0.596	7.01	2.45	58.7

[a] Au-NP/V_2O_5 indicates that the as-synthesized Au-NP solution was spin-coated onto the ITO substrate before V_2O_5 layer deposition. [b] Au-NP:PSS indicates that 0.2 wt% PSS-mixed Au-NP solution was spin-coated onto the ITO substrate before V_2O_5 layer deposition.

Table 2 Extracted parameters from dark current–voltage characteristics of the P3HT:$PC_{61}BM$ solar cells

Buffer layer	J_s (μA cm^{-2})	R_s (Ω cm^2)	R_p (Ω cm^2)	n
V_2O_5	0.8	1.2	700	1.8
Au-NP/V_2O_5[a]	0.62	1.3	200	1.8
Au-NP:PSS[b]/V_2O_5	0.15	0.60	2500	1.9

[a] Au-NP/V_2O_5 indicates that the as-synthesized Au-NP solution was spin-coated onto the ITO substrate before V_2O_5 layer deposition. [b] Au-NP:PSS indicates that 0.2 wt% PSS-mixed Au-NP solution was spin-coated onto the ITO substrate before V_2O_5 layer deposition.

58.7% for the V_2O_5 buffer and Au-NP:PSS/V_2O_5 bilayer buffer, respectively. The enhancement in the fill factor indicates an improvement of the charge transport properties induced by the incorporated Au-NP:PSS layer. A similar J_{sc} value indicates that Au-NPs do not have a pronounced effect on the optical absorption in the photoactive layer, which is confirmed by the IPCE spectra and UV-visible absorption spectra of various buffer layers (Fig. 3(b)).

IPCE is commonly used to demonstrate the presence of the plasmonic effect from noble metallic nanoparticles, which could cause significant absorption enhancement at wavelengths

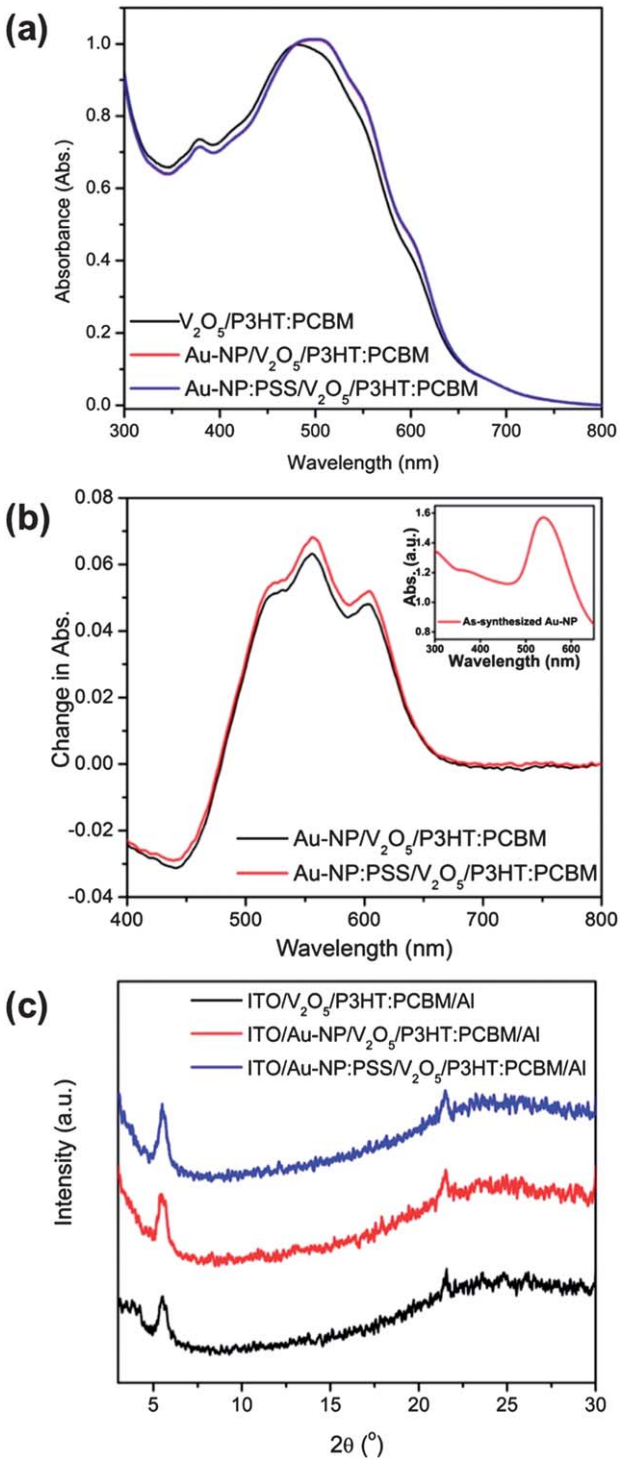

Fig. 5 (a) UV-visible absorption spectra of P3HT:$PC_{61}BM$ polymer solar cells with (black) V_2O_5, (red) Au-NP/V_2O_5, and (blue) Au-NP:PSS/V_2O_5 respectively, (b) absorption change (ΔAbs) of polymer solar cells after incorporating Au-NPs (black line) and Au-NP:PSS (red line) in the devices' anodic buffer layer and (c) XRD spectra of polymer solar cell with (black) V_2O_5, (red) Au-NP/V_2O_5, and (blue) Au-NP:PSS/V_2O_5. (The peak at $2\theta = 22°$ is from ITO).

ranging from around 450 nm to 600 nm,[21] corresponding to the LSPR range of metallic nanoparticles. The IPCE curves of devices with the V_2O_5 buffer and Au-NP:PSS/V_2O_5 bilayer buffer in Fig. 3(b) show similar shapes and intensity throughout the visible light wavelengths. This result is in good agreement with the similar J_{sc} values of the two devices, as shown in Table 1. As such, the IPCE results demonstrate that the plasmonic effect is probably absent in the device with the Au-NP layer. In addition, the UV-visible absorption spectra of various buffer layers were examined to investigate the plasmonic contribution from Au-NP layer. As shown in the inset of Fig. 3(b), incorporating Au-NP underneath the V_2O_5 buffer layer has no discernible effect on the absorption spectrum of the buffer layer at wavelengths ranging from 450 nm to 600 nm. Based on the current IPCE and UV-visible absorbance results, we conclude that the insertion of a low density Au-NP:PSS layer does not induce optical absorption enhancement.

It should be noted that in this work, PSS is mixed with Au-NPs to create a more uniform distribution of Au-NPs on the ITO substrate. In order to investigate the effects of PSS on the device performance, a PSS-only device was fabricated in which only PSS was deposited at the interface of ITO substrate and V_2O_5 buffer layer. The concentration of PSS used for spin coating on the ITO substrate was 2 mg ml^{-1}, which is the same as the amount of PSS mixed with the as-prepared Au-NP solution. As shown in Fig. S3,† the PSS-only device shows similar *J–V* characteristica and PCE as the reference devices. We thus conclude that PSS itself does not exert a discernible effect on the device performance.

To gain a better understanding of the performance enhancement by the addition of the Au-NP:PSS layer, the internal resistance of the polymer solar cell was extracted using an equivalent circuit model (inset of Fig. 4(a)) by fitting the experimental results under dark conditions (Fig. 4(a)) using a modified vertical optimization method.[28–30] From the equivalent circuit, the current density (J) *versus* applied voltage (V) can be described using the generalized Shockley equation.[31]

$$J = \frac{R_p}{R_p + R_s}\left\{J_s\left[\exp\left(\frac{q(V - JR_s)}{nk_BT}\right) - 1\right] + \frac{V}{R_p}\right\} \quad (1)$$

where R_p is the parallel resistance, R_s is the serial resistance, n is the ideality factor, and J_s represents the reverse dark saturation current density when it is biased with a negative voltage.

The extracted parameters summarized in Table 2 show that the reference cell (P3HT:$PC_{61}BM$ polymer solar cell with V_2O_5 buffer layer) has low R_p (700 Ω cm^2), high R_s (1.2 Ω cm^2) and high J_s (0.8 μA cm^{-2}). On the other hand, the polymer solar cell with the Au-NP:PSS/V_2O_5 bilayer buffer has R_p increased by a factor of 3 (from 700 Ω cm^2 to 2500 Ω cm^2), and R_s reduced by a factor of 2 (from 1.2 Ω cm^2 to 0.6 Ω cm^2) compared with the reference cell. The improvement in the internal resistance is in agreement with the higher fill factor, which could be ascribed to the reduction of the charge transport resistance (evident from the reduction in R_s) resulting from better electrical conductivity due to the more uniformly distributed Au-NP/V_2O_5 bilayer buffer. In addition, higher recombination resistance (evident from the increase in R_p) minimizes the occurrence of charge recombination and thus leads to higher PCE.

To further evaluate the charge transport properties across the anodic buffer layer/P3HT interface, hole-only devices with

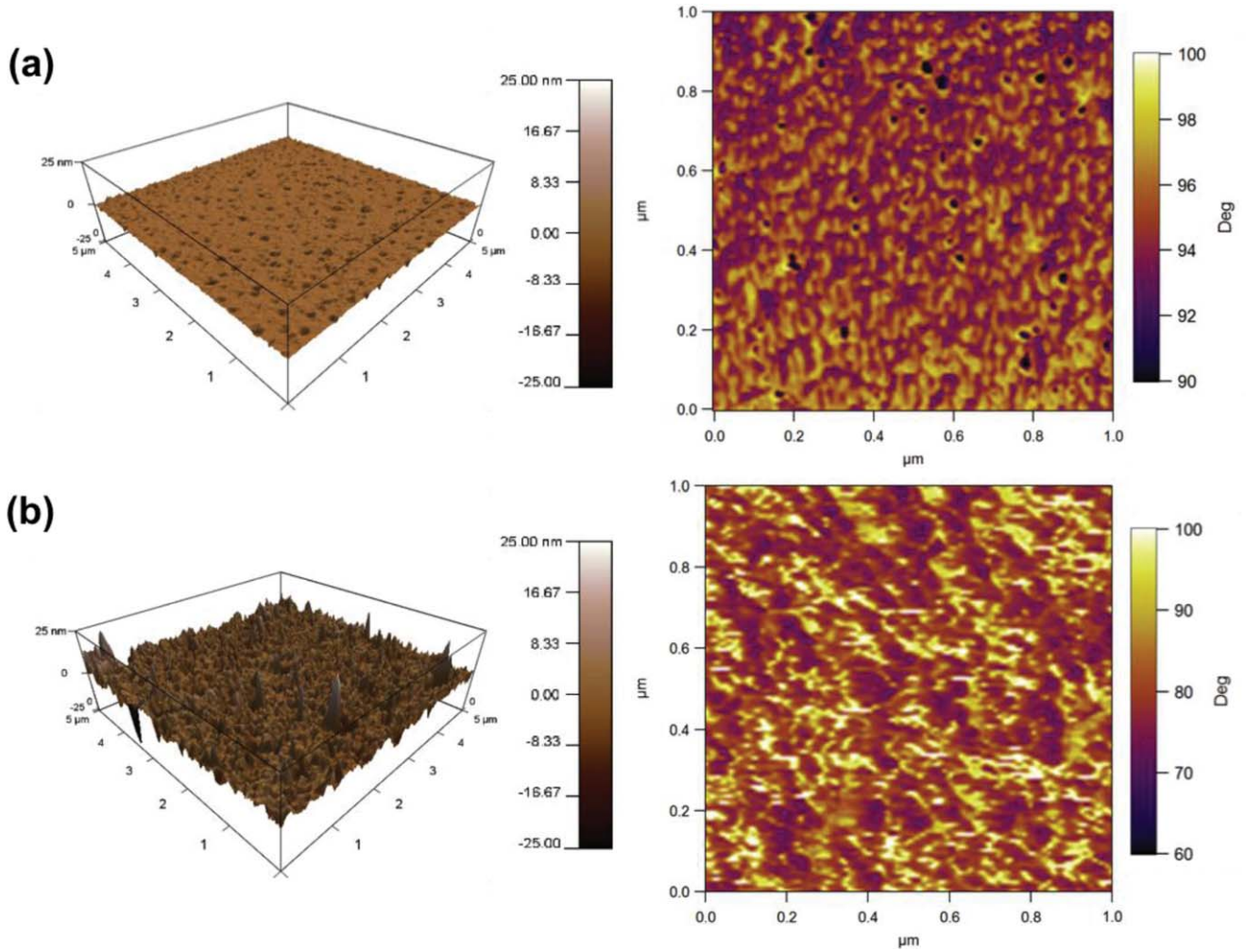

Fig. 6 Tapping-mode AFM images of the P3HT:$PC_{61}BM$ active layer (without aluminium electrode): (left) 3D height image and (right) 2D phase diagram of the active layer with (a) V_2O_5 and (b) Au-NP:PSS/V_2O_5 as the anodic buffer layer.

different anodic buffer layers, namely ITO/V_2O_5/P3HT/Au, ITO/Au-NP/V_2O_5/P3HT/Au and ITO/Au-NP:PSS/V_2O_5/P3HT/Au, were fabricated. The *J–V* characteristics of the hole-only devices for various anodic buffer layers are shown in Fig. 4(b). A curved *J–V* line is observed for the hole-only device with the Au-NP/V_2O_5 bilayer buffer indicating that the performance of the polymer solar cell is limited by the space-charged limited current, which is in agreement with the lower fill factor, V_{oc} and PCE. Linear and symmetric *J–V* relationships were observed for the P3HT hole-only devices with V_2O_5 and Au-NP:PSS/V_2O_5 bilayer anodic buffer which implies that the V_2O_5 and Au-NP:PSS/V_2O_5 buffer layers provide true ohmic contact for the polymer solar cell at the anodic buffer and polymer active interface,[32] in which the ohmic contact could account for the higher V_{oc} of the devices. Moreover, the current density of the hole-only device with the Au-NP:PSS/V_2O_5 bilayer buffer is two times higher than that of the reference cell, which implies a smaller series resistance of the Au-NP:PSS/V_2O_5 device. These results illustrate that the insertion of the Au-NP:PSS layer effectively enhances the electrical conductivity of the polymer solar cell.

The effects of Au-NPs on the photoactive layer were further investigated by UV-visible spectrometry, XRD and tapping-mode AFM. Fig. 5(a) shows the absorption spectra of the P3HT:$PC_{61}BM$ active layer on V_2O_5 with or without the insertion of Au-NPs, while Fig. 5(b) displays the change of the UV-visible absorbance spectrum of the active layer after the insertion of Au-NPs, in which the change is calculated by subtracting the absorption spectrum of the photoactive layer after Au-NP insertion from the absorption spectrum of photoactive layer with the V_2O_5 buffer layer only. The possibility of an increase in the UV-visible absorption spectrum induced by plasmonic contributions from the incorporated Au-NPs is eliminated, as the curve of the UV-visible absorbance spectrum of the as-synthesized Au-NP solution (inset of Fig. 5(b)) is different from the change in the UV-visible absorption spectrum after the insertion of Au-NPs (as shown in Fig. 5(b)). The UV-visible absorption spectra of the active layer with Au-NP/V_2O_5 and Au-NP:PSS/V_2O_5 bilayer anodic buffer are overlapping, in which vibronic structure with peaks at 530 nm and 610 nm, and a gradually increasing and broadening peak located at around

500 nm is observed in the absorption spectra of the active layer with Au-NP/V_2O_5 and Au-NP:PSS/V_2O_5 bilayer anodic buffer, as shown in Fig. 5(a). The increase in the intensity of the absorption peak at 530 nm indicates the enhancement in intrinsic π–π^* transitions of P3HT and the peak located at 610 nm corresponds to the enhancement of the 0–0 vibronic transition of planarized P3HT, which indicates strong interchain-interlayer interactions among the P3HT chains and good polymer ordering in the blend films.[33–38] The XRD patterns of various P3HT:$PC_{61}BM$ active layers further confirms the results from the UV-visible measurements. The peak at $2\theta \approx 5.6^\circ$ shown in Fig. 5(c) corresponds to the interchain spacing in P3HT associated with interdigitated alkyl chains.[38–40] In comparison with that of the polymer solar cell with the V_2O_5 buffer layer only, a higher intensity is observed for the peaks at $2\theta \approx 5.6^\circ$ for the P3HT:$PC_{61}BM$ active layer on the Au-NP:PSS/V_2O_5 buffer, which may imply a higher degree of P3HT crystallinity in the P3HT:$PC_{61}BM$ active layer.

The effect of Au-NPs on the morphology of the photoactive layer was further examined with AFM. The morphology was obtained from complete devices by detaching the Al electrode using scotch tape.[6,38,41] As shown in Fig. 6, the surface roughness of the photoactive layer increased dramatically and the root mean square roughness increased from 0.580 nm to 4.124 nm for devices with the V_2O_5 buffer and Au-NP:PSS/V_2O_5 bilayer buffer, respectively. The increase in the photoactive layer surface roughness could be considered a signature of polymer self-organization resulting from enhanced ordered structure formation in the thin film, which has been independently reported in various articles.[6,38,42] This observation suggests that the Au-NP:PSS layer induced higher P3HT crystallinity and enhanced the contact interaction with the Al electrode,[38] which led to the reduction of the device's charge transfer resistance and thus resulted in the increase of the fill factor. Besides the height profile, the phase diagrams of the active layers from the V_2O_5 and Au-NP:PSS/V_2O_5 bilayer buffer also show significant differences. As shown in Fig. 6(a), the phase diagram of the photoactive layer with the V_2O_5 buffer shows an homogenous phase with a lack of phase contrast, which indicates more amorphous characteristics of the as-cast P3HT and $PC_{61}BM$.[43] On the contrary, larger phase contrast (as displayed in Fig. 6(b)) is observed for the active layer with the Au-NP:PSS/V_2O_5 bilayer. This indicates the formation of good crystallinity and an interfusion network within the bulk heterojunction region, which are beneficial for exciton dissociation. We suggest that the protrusion point, which is caused by the insertion of the Au-NP:PSS layer, induced the alignment of P3HT within the phase-separated networks, hence resulting in the improvement of the charge transport to the electrodes.[12,29,44]

Conclusions

The current work investigates the PCE enhancement mechanism of polymer solar cells by uniformly distributing Au-NPs in the buffer layer. Our studies eliminate the possibility of PCE enhancement from the Au-NPs' plasmonic effects, while indicating a significant charge extraction improvement attributed to possible enhanced crystallinity of the active layer and interfacial charge transfer. This work also demonstrates that besides the plasmonic effect, the role of Au-NPs in the electrical characteristics and crystalline structure of the photovoltaic devices should also be considered in the performance improvement of bulk-heterojunction polymer solar cells.

Acknowledgements

This work is financially supported by a research grant from the Agency for Science, Technology and Research (A*STAR) under SERC grant no. 102 170 0142. Other forms of support from Nanyang Technological University and GlobalFoundries Singapore Pte. Ltd are also acknowledged.

Notes and references

1 Y.-M. Chang and L. Wang, *J. Phys. Chem. C*, 2008, **112**, 17716–17720.
2 C. W. Tang, *Appl. Phys. Lett.*, 1986, **48**, 183–185.
3 K. X. Steirer, J. J. Berry, M. O. Reese, M. F. A. M. van Hest, A. Miedaner, M. W. Liberatore, R. T. Collins and D. S. Ginley, *Thin Solid Films*, 2009, **517**, 2781–2786.
4 H. Zhou, Y. Zhang, J. Seifter, S. D. Collins, C. Luo, G. C. Bazan, T.-Q. Nguyen and A. J. Heeger, *Adv. Mater.*, 2013, **25**, 1646–1652.
5 J. S. Moon, C. J. Takacs, S. Cho, R. C. Coffin, H. Kim, G. C. Bazan and A. J. Heeger, *Nano Lett.*, 2010, **10**, 4005–4008.
6 G. Li, V. Shrotriya, J. Huang, Y. Yao, T. Moriarty, K. Emery and Y. Yang, *Nat. Mater.*, 2005, **4**, 864–868.
7 J. Peet, M. L. Senatore, A. J. Heeger and G. C. Bazan, *Adv. Mater.*, 2009, **21**, 1521–1527.
8 Z. He, C. Zhong, S. Su, M. Xu, H. Wu and Y. Cao, *Nat. Photonics*, 2012, **6**, 593–597.
9 H.-L. Yip and A. K.-Y. Jen, *Energy Environ. Sci.*, 2012, **5**, 5994–6011.
10 T. V. Pho, P. Zalar, A. Garcia, T.-Q. Nguyen and F. Wudl, *Chem. Commun.*, 2010, **46**, 8210–8212.
11 S. Murase and Y. Yang, *Adv. Mater.*, 2012, **24**, 2459–2462.
12 B. Peng, X. Guo, C. Cui, Y. Zou, C. Pan and Y. Li, *Appl. Phys. Lett.*, 2011, **98**, 243308–243303.
13 S. Chen, J. R. Manders, S.-W. Tsang and F. So, *J. Mater. Chem.*, 2012, **22**, 24202–24212.
14 H. Shen, P. Bienstman and B. Maes, *J. Appl. Phys.*, 2009, **106**, 073109–073105.
15 W.-J. Yoon, K.-Y. Jung, J. Liu, T. Duraisamy, R. Revur, F. L. Teixeira, S. Sengupta and P. R. Berger, *Sol. Energy Mater. Sol. Cells*, 2010, **94**, 128–132.
16 J. Wang, Y.-J. Lee, A. S. Chadha, J. Yi, M. L. Jespersen, J. J. Kelley, H. M. Nguyen, M. Nimmo, A. V. Malko, R. A. Vaia, W. Zhou and J. W. P. Hsu, *J. Phys. Chem. C*, 2012, **117**, 85–91.
17 M. Heo, H. Cho, J.-W. Jung, J.-R. Jeong, S. Park and J. Y. Kim, *Adv. Mater.*, 2011, **23**, 5689–5693.
18 J. Yang, J. You, C.-C. Chen, W.-C. Hsu, H.-r. Tan, X. W. Zhang, Z. Hong and Y. Yang, *ACS Nano*, 2011, **5**, 6210–6217.

19 J. Ye, K. Bonroy, D. Nelis, F. Frederix, J. D'Haen, G. Maes and G. Borghs, *Colloids Surf., A*, 2008, **321**, 313–317.
20 H. A. Atwater and A. Polman, *Nat. Mater.*, 2010, **9**, 205–213.
21 J.-L. Wu, F.-C. Chen, Y.-S. Hsiao, F.-C. Chien, P. Chen, C.-H. Kuo, M. H. Huang and C.-S. Hsu, *ACS Nano*, 2011, **5**, 959–967.
22 D. H. Wang, D. Y. Kim, K. W. Choi, J. H. Seo, S. H. Im, J. H. Park, O. O. Park and A. J. Heeger, *Angew. Chem., Int. Ed.*, 2011, **50**, 5519–5523.
23 J. Kimling, M. Maier, B. Okenve, V. Kotaidis, H. Ballot and A. Plech, *J. Phys. Chem. B*, 2006, **110**, 15700–15707.
24 K. Zilberberg, S. Trost, H. Schmidt and T. Riedl, *Adv. Energy Mater.*, 2011, 377–381.
25 X. Ji, X. Song, J. Li, Y. Bai, W. Yang and X. Peng, *J. Am. Chem. Soc.*, 2007, **129**, 13939–13948.
26 S. S. Kumar, C. S. Kumar, J. Mathiyarasu and K. L. Phani, *Langmuir*, 2007, **23**, 3401–3408.
27 J. Cho and F. Caruso, *Chem. Mater.*, 2005, **17**, 4547–4553.
28 A. Ferhat-Hamida, Z. Ouennoughi, A. Hoffmann and R. Weiss, *Solid-State Electron.*, 2002, **46**, 615–619.
29 C. Gong, H. B. Yang, Q. L. Song, Z. S. Lu and C. M. Li, *Sol. Energy Mater. Sol. Cells*, 2012, **100**, 115–119.
30 H. Yang, C. Gong, G. Hong Guai and C. Ming Li, *Sol. Energy Mater. Sol. Cells*, 2012, **101**, 256–261.
31 N. Li, B. E. Lassiter, R. R. Lunt, G. Wei and S. R. Forrest, *Appl. Phys. Lett.*, 2009, **94**, 023307–023303.
32 J. T. Lim, J. W. Kwon and G. Y. Yeom, *J. Electrochem. Soc.*, 2011, **158**, J10–J14.
33 H. Yamagata and F. C. Spano, *J. Chem. Phys.*, 2012, **136**, 184901–184914.
34 G. Li, Y. Yao, H. Yang, V. Shrotriya, G. Yang and Y. Yang, *Adv. Funct. Mater.*, 2007, **17**, 1636–1644.
35 R. A. Marsh, J. M. Hodgkiss, S. Albert-Seifried and R. H. Friend, *Nano Lett.*, 2010, **10**, 923–930.
36 J. Clark, C. Silva, R. H. Friend and F. C. Spano, *Phys. Rev. Lett.*, 2007, **98**, 206406.
37 F. C. Spano, *J. Chem. Phys.*, 2005, **122**, 234701–234715.
38 W. Ma, C. Yang, X. Gong, K. Lee and A. J. Heeger, *Adv. Funct. Mater.*, 2005, **15**, 1617–1622.
39 T. Erb, U. Zhokhavets, G. Gobsch, S. Raleva, B. Stühn, P. Schilinsky, C. Waldauf and C. J. Brabec, *Adv. Funct. Mater.*, 2005, **15**, 1193–1196.
40 T.-A. Chen, X. Wu and R. D. Rieke, *J. Am. Chem. Soc.*, 1995, **117**, 233–244.
41 P. Peumans, S. Uchida and S. R. Forrest, *Nature*, 2003, **425**, 158–162.
42 H. Yang, Q. Song, Z. Lu, C. Guo, C. Gong, W. Hu and C. M. Li, *Energy Environ. Sci.*, 2010, **3**, 1580–1586.
43 A. L. Ayzner, C. J. Tassone, S. H. Tolbert and B. J. Schwartz, *J. Phys. Chem. C*, 2009, **113**, 20050–20060.
44 R. A. Marsh, C. Groves and N. C. Greenham, *J. Appl. Phys.*, 2007, **101**, 083509–083507.